Atmos. Chem. Phys. Discuss., 14, 8393–8418, 2014
www.atmos-chem-phys-discuss.net/14/8393/2014/
doi:10.5194/acpd-14-8393-2014

Atmospheric Chemistry and Physics Discussions

Mesoscopic surface roughness of ice crystals pervasive across a wide range of ice crystal conditions

N. B. Magee, A. Miller, M. Amaral, and A. Cumiskey

The College of New Jersey, Ewing, NJ

Received: 19 December 2013 – Accepted: 19 February 2014 – Published: 28 March 2014

Correspondence to: N. B. Magee (magee@tcnj.com)

Published by Copernicus Publications on behalf of the European Geosciences Union.

Abstract

Here we show high-magnification images of hexagonal ice crystals acquired by Environmental Scanning Electron Microscopy (ESEM). Most ice crystals were grown and sublimated in the water vapor environment of an FEI-Quanta-200 ESEM, but crystals grown in a laboratory diffusion chamber were also transferred intact and imaged via ESEM. All of these images display prominent mesoscopic topography including linear striations, ridges, islands, steps, peaks, pits, and crevasses; the roughness is not observed to be confined to prism facets. The observations represent the most highly magnified images of ice surfaces yet reported and expand the range of conditions where the rough surface features are known to be conspicuous. Microscale surface topography is seen to be ubiquitously present at temperatures ranging from −10 °C to −40 °C, at super-saturated and sub-saturated conditions, on all crystal facets, and irrespective of substrate. Despite the constant presence of surface roughness, the patterns of roughness are observed to be dramatically different between growing and sublimating crystals, and transferred crystals also display qualitatively different patterns of roughness. Crystals are also demonstrated to sometimes exhibit inhibited growth in moderately supersaturated conditions following exposure to near-equilibrium conditions, a phenomena interpreted as evidence of 2-D nucleation. New knowledge of the characteristics of these features could affect the fundamental understanding of ice surfaces and their physical parameterization in the context of satellite retrievals and cloud modeling. Links to Supplement videos of ice growth and sublimation are provided.

1 Introduction

It has been broadly recognized (IPCC, 2007; Bony et al., 2006) that cloud-climate feedbacks are the most weakly constrained radiative forcings for general circulation models of a changing future climate. Among the variety of cloud feedbacks that have been identified and parameterized, cirrus clouds are notable for being especially uncertain

ACPD
14, 8393–8418, 2014

– even the sign of the likely feedback effect is subject to debate (Mitchell et al., 2008; Burkhardt, 2011). Baran (2012) presents a compelling case that the complex radiative scattering properties of hetereomorphic ice crystals must be accounted for in order to reach a physically consistent parameterization of ice clouds in climate models. In addition to cloud-climate feedbacks, it is expected that prominent mesoscopic topography would affect active research questions in statospheric ozone chemistry (McNeill et al., 2007) and thunderstorm electrification (Dash et al., 2001). Despite recognition that the microscale structures of ice are critically important to consider, very few images of ice are available at this resolution.

While many experimental research efforts have characterized the effects of temperature, supersaturation, and pressure on particle-scale ice crystal growth rates and morphology under conditions relevant to atmospheric processes (Lamb and Hobbs, 1971; Kuroda and Lacmann, 1982; Bailey and Hallet, 2004; Nelson and Knight, 1998; Magee et al., 2006), to date the limits of light microscopy have prevented a thorough analysis of the surface details of ice crystals beyond the microscale. Several studies have employed interference techniques or ellipsometry to suggest the presence of surface structure and disorder of ice (Bryant et al., 1960; Furukawa et al., 1987; Sazaki et al., 2010), but no highly-resolved images of mesoscopic surface structure have been available. The first SEM images of ice were made from platinum sputter-coated natural snowflakes by Wergin et al. (1995); their striking images show a variety of complex structures, but due to warm collection conditions and the sputtering processes, they are ambiguous with respect to presence of mesoscopic surface structure (Wergin et al., 1995). Recently, Neshyba et al. (2013), Ulanowski et al. (2013), Petersen et al. (2011), Pfalzgraff et al. (2010), Kuhs et al., 2010, and Zimmerman et al. (2007) have used uncoated, in-situ growth of ice crystals in ESEM or VPSEM to identify surface roughness in the form of ridges or "trans-prismatic" strands. Through images resolved at up to 10 000× magnification (compared with previous maximum magnifications of ∼ 1000×), our observations underscore this newly emerging view of the ice surface, demonstrating that mesoscopic surface roughness is a non-uniform

ACPD
14, 8393–8418, 2014

condition present on a wide array of ice crystals, and is not confined to a narrow range of macroscopic morphology, substrate, temperature, humidity, or growth rates.

Over fifty years have passed since the first account of a relationship between surface roughness and specular reflectivity (Bennett and Porteus, 1961). A growing recognition is now emerging that divergence away from the classical smooth-facet assumption for ice will affect the way that light is scattered. A broad suite of recent measurements and models describe the potential effect of surface roughness and complex micro-scale geometry in smoothing the peaks of the ice-scattering phase function (Baran, 2012; Baum et al., 2010, 2011; Cotton et al., 2010; Heymsfield et al., 2006; Ulanowski et al., 2006, 2010, 2012; Um and McFarquhar, 2011).

Despite acknowledged uncertainty regarding the details of real roughened ice surfaces, a variety of recent studies have concluded that cirrus radiative measurements and models come into better agreement when attempting to account for complicated shapes and rough ice surfaces. For example, Kahnert et al. (2008) estimated that the effect of varying parameterizations of ice surface microphysics can affect the modeled radiative influence of cirrus by a factor of two. Baum et al. (2011) recently determined that assumption of a roughened ice surface results in better fits to ice particle data retrievals from the CALIOP lidar instrument on board the NASA-CALIPSO A-train satellite. Mauno et al. also point out discrepancies between measured and modeled cirrus-modulated shortwave radiative fluxes that would be improved by assumption of surface roughness on ice crystals (Mauno, 2011). In addition to passive satellite measurements of cirrus ice microphysics, it is also likely that ice scattering functions assumed in radar and lidar imaging of cirrus and mixed-phase cloud properties would be affected (Sun et al., 2011). Because satellite observations, aircraft measurements, and modeling of cirrus and mixed-phase clouds have often been at odds (Baran, 2012; Garrett and Gerber, 2003; Gierens et al., 2003; Kramer et al., 2009; Harrington et al., 2009; Jensen et al., 2009; McFarquhar et al., 2007; Peter et al., 2006; Connolly et al., 2007), potential artifacts of surface roughness on both satellite retrievals and modeling of ice microphysics must be carefully evaluated.

ACPD
14, 8393–8418, 2014

2 Methods

We employed an FEI Quanta-200 FEG environmental scanning electron microscope (ESEM) to observe ice crystals at temperatures from −10 °C to −45 °C and through a wide range of under-saturated, equilibrium, and super-saturated vapor pressures. Most experiments examined in-situ nucleation, growth, and sublimation of ice crystals in the pure water vapor environment of the ESEM. Several experiments also included imaging of ice crystals grown in an external diffusion chamber and then transferred into the ESEM.

2.1 In-situ growth and sublimation

In-situ growth and sublimation experiments were conducted on the ESEM stage, with the ice nucleating on a substrate mounted to a Peltier cooling block. An aluminum stub fitted to the Peltier block was machined to expose a 1 mm diameter surface to the chamber environment such that the entire surface could be contained in the ESEM field of view at low magnification. An insulating vinyl mask was used to ensure that ice growth was limited to the intended cold surface. Growth and sublimation experiments were conducted on bare aluminum as well as on a variety of thin substrates that were attached to the aluminum by thermally conductive epoxy. Substrates that were tested included stainless steel, aluminum, and copper, as well as mineral substrates including Covellite, Muscovite, Bismuth, Magnesite, Galena, and Quartz.

Once the substrate was mounted onto the Peltier stage, the ambient air in the ESEM chamber was evacuated and back-filled with water vapor, after which the ice growth experiments were initiated. After cooling to a temperature at or above −45 °C, ice nucleation, growth, and sublimation was controlled through direct adjustment of the water vapor pressure or surface temperature. Vapor pressure was controlled at 0.5 Pa increments between 0 and 500 Pa via automatic differential pumping. Vapor measurements were made to 0.1 Pa resolution. In a typical experiment, vapor pressure was first adjusted to the equilibrium frost point and subsequently increased in small increments

ACPD
14, 8393–8418, 2014

until ice crystal nucleation was observed. A magnification of 100× was employed until ice crystal growth became visible, after which variable resolutions (as high as about 10 000×) were used in order to capture detailed images and movies of the growing ice crystals. Maximum image aquisition size for the FEI Quanta200 is 4096 × 3775 pixels (∼ 15.5 MP). At 2500× magnification, this results in a single pixel with dimension 25.4 nm × 25.4 nm. At 2500× magnification, we observed that typical imaging conditions resulted in linear features that could be resolved at limits of 23 pixels (50–75 nm). With increasing magnification further, signal-to-noise reduction partially (but not completely) offset resolution gains, such that we estimate a resolution limit of approximately 25 nm for these methods.

In a typical experiment, the differential pumping and thermoelectric cooling of the substrate required approximately 10 min to reach equilibrium values of vapor pressure near 65 Pa and −25 °C. Temperature of the Peltier block is automatically reported through the FEI instrument software to 0.1 °C resolution and the water vapor pressure is reported to 0.1 Pa resolution. We are confident that vapor pressure values were precisely and accurately controlled and reported; however, we determined that the surface temperature of the substrate was 2 ± 0.5 °C warmer than the temperature indicated for the Peltier base. This offset was determined by observing the (equilibrium) vapor pressure at which ice neither grew nor sublimated and inferring surface temperature from the Murphy and Koop vapor pressure formulation (2005); we observed this thermal offset to vary slightly based on the thickness of the substrate and its thermal conductivity. Following the approach to equilibrium, vapor pressure was raised in 0.5 Pa increments until nucleation of one or several ice crystals occurred. It was frequently challenging to nucleate a single crystal, even with incremental increases in vapor pressure. Once a crystal of interest was developed, it was examined and photographed at a variety of magnifications, ranging from 100× to 10 000× and at a variety of vapor densities, including super- and sub-saturated conditions, and through multiple cycles of growth and sublimation.

ACPD
14, 8393–8418, 2014

2.2 Transported crystals

Ice crystals were grown in a diffusion chamber contained within a large-volume, ultra-low temperature freezer. Ice crystals were grown at ambient lab pressure (~ 1000 hPa), and at low supersaturation (< 110 % RH_i), with temperature near −50 C. Within the freezer, these ice crystals were then captured in a pre-chilled small-volume (~ 1 cm^3) containment cell. The base of the containment cell was formed from an aluminum stub to allow direct transfer into the ESEM cooling stage. Upon capture, the cell was sealed closed and transferred to a specially-designed cryogenic dewer (filled with liquid nitrogen or crushed dry ice) for transport to the ESEM. The cell was then removed from the dewer and quickly placed onto the pre-chilled cooling stage of the ESEM. Throughout the capture and transfer process, the primary objective was to allow ESEM imaging of the ice surfaces as they had been growing in the diffusion chamber and without additional sublimation or growth. To prevent unintended sublimation, the small-volume containment cell was filled with many crystals and quickly sealed so that equilibrium vapor pressures would preserve the crystal surfaces. The containment cell was also enveloped by materials with significant heat capacity and the cryo-dewer designed and handled to maintain near isothermal conditions. Once the sealed containment cell was transferred to the ESEM cooling stage, the microscope chamber was evacuated and adjusted to equilibrium vapor pressures matching the cold stage and containment cell temperature. After reaching equilibrium vapor pressure in the ESEM chamber, the containment cell was then opened using electronically driven stage movement to mechanically pull off the top seal. Following unsealing of the containment cell, ESEM imaging could proceed as in the in-situ growth and sublimation experiments.

3 Results and discussion

The overriding impression of our experiments suggests that surface structures on the 0.1 to 10 micron scale are a ubiquitous feature of ice crystal facets. The morphology

ACPD
14, 8393–8418, 2014

of many of these structures agree with observations recently reported by Neshyba et al. (2013), Ulanowski et al. (2013), Pfalzgraff et al. (2010), Petersen et al. (2011), and Zimmerman et al. (2007). Our observations provide new evidence of roughening on basal crystal facets, as well as images and videos at high magnifications (1000×–10 000×) that reveal smaller scale roughening that is not readily apparent at magnification below 1000×. Our observations also show strongly different morphology between textures of growing surfaces as compared to sublimating surfaces. The results also include images of ice crystals grown in air–vapor mixtures. These images do show mesoscopic surface roughness, but suggest that the presence of air or different modes of internal heat transfer may significantly affect the character of surface texture development.

3.1 Growing crystals

As described in Sect. 2.1, ice crystals where nucleated and grown on an ESEM cold state at a variety of temperatures and pressues. Crystals typically nucleated at just a few percent above equilibrium vapor pressures and continued to grow steadily in proportion to the magnitude of ice supersaturation. At high supersaturations > 150 % RH_i, nucleation and growth proceeded so quickly that it was difficult to isolate and follow the progression of a single crystal, as the entire stage would be overtaken by intersecting crystals within a few seconds. Therefore, most growth experiments occured at modest supersaturation, usually 105–125 % RH_i. While we did observe clear surface morphology differences between growing and sublimating crystals, we did not detect a systematic dependence on the degree of supersaturation or the rate of growth.

3.1.1 Roughness morphologies and scales

In our ESEM growth experiments, we observed mesoscopic linear striations on prism faces (Fig. 1e–g) similar to those described by Neshyba et al. (2013) and Pfalzgraff et al. (2010) as well as a variety of other mesoscopic roughness structures. Figure 1

ACPD
14, 8393–8418, 2014

provides a multi-panel view of characteristic growing surface features across the range of our roughness obserations. The panels are organized with temperature decreasing toward the bottom and magnification increasing to the right of the figure.

Particularly in Fig. 1a, c, d, f, and g, distinct roughness can be observed on the basal facets of growing crystals as well as the prism facets. The basal plane roughess usually appears less linear and less symmetrically organized than the prismatic strands. Image sequences (typically around 1 frame s^{-1}) reveal the dynamic progress of roughening features as they migrate across the ice surface (videos available in Supplement data). Figure 1g–i also displays evidence of microfaceting on basal and prism facets. Microfaceting could be induced by cycles of growth and submlimation at all temperatures, but was only observed to develop during steady growth at temperatures below −35 °C.

These data have also confirmed the idea that surface roughness can be enhanced in proximity to a grain boundary between two neighboring crystals (e.g. Pedersen et al., 2011). In Fig. 1b, it is apparent that the ridges (in the centers of the images) become larger just as the two advancing facets collide, with ridges radiating outward from the impact point. A video of ridge topographic intensification precipitated by colliding ice crystals is available in the Supplement. Blackford (2007) and Pedersen et al. (2011) point out that the microstructure of ice along grain boundaries can play an important role in advancing the understanding of the mechanical properties of snowpacks that are susceptible to avalanche, as well as the dynamics of glaciers.

3.1.2 Magnification and contrast effect

Figure 2 shows a four-panel plot of a growing hexagonal ice crystal starting at 762× magnification in Fig. 2a. This crystal was grown near −23 °C and is being held at equilibrium in this sequence of panels; the crystal was not visibly growing or sublimating across the 57 s separating the first and final panel. Mesoscopic topography is not visible in Fig. 2a, so the magnification was increased to 2155× (Fig. 2b), which made roughness apparent on the prism facets of the ice crystals. However, the basal facet

ACPD
14, 8393–8418, 2014

is tilted almost perpendicular to our viewing angle; therefore, we could not see if any complex surface architecture existed on the basal facet. By increasing the magnification further and adjusting the contrast and brightness of the ESEM, Fig. 2c shows that rough surface topography was actually present on the basal facet (at 3625× magnification). A measurement was made of the depth of a prominent terrace in Fig. 2d (1.59 microns); this terrace is among the thickest observed during experiments, suggesting that most topographic features have heights well below 1 micron. This pattern was typical of all experiments; only the most prominent surface structures were typically visible at a magnification of 500×–1000×, while closer examination at 1000–5000× would reveal smaller-scale structures and topography on surfaces that had not been resolved at lower magnification, aspect, or sub-optimal brightness and contrast.

We attempted to extract profiles of surface height from our ESEM micrographs in order to calculate the roughness measure $\langle r \rangle$ recently defined by Neshyba et al. (2013) in the context of carefully meaured mesoscopic striations observed on ice prism facets growing in VPSEM at −45 °C:

$$r = 1 - \sqrt{\frac{1}{1 + \left(\frac{dy}{dz}\right)^2}}. \quad (1)$$

The average roughness $\langle r \rangle$ is then determined along the measured profile. In several circumstances, we succeeded in retrieving an approximate profile, but, as indicated by Ulanowski et al. (2013), in most routine SEM imaging circumstances, we found that it was not straightforward to extract this height profile with confidence. Where this profile could be estimating on growing crystals imaged at magnifications similar to those analyzed by Neshyba et al. (∼ 300–500× magnification), we retrieved similar values of roughness near $\langle r \rangle \approx 0.05$. Height profiles along several sections of more highly magnified crystals indicated by red rectangles in Fig. 1f and i yielded $\langle r \rangle$ between 0.10 and 0.40. Height profiles, and thereby $\langle r \rangle$ values, can be retrieved by careful attention during the imaging process to SEM stage and crystallographic orientation, resolving

ACPD
14, 8393–8418, 2014

of crystal edges, or potentially by 3-D reconstruction of equilibrium crystals captured from multiple angles. We found that it was usually not possible to determine height profiles when structures are visible, but near the limit of the image resolution, or where pronounced roughness did not intersect a resolved crystal edge, a common feature in our observations. We also find that the $\langle r \rangle$ metric, much like the subjective perception of roughness, is affected by image magnification and resolution, and in-turn by the minimum sampling interval of the height profile. If, as our observations imply, surface roughness is significant at sub-micron scales that are not well-resolved at 500× magnification, $\langle r \rangle$ values obtained from profiles retrieved at 500× may be underestimating total roughness.

3.1.3 Inhibited growth observations

As expected, with growth experiments occuring on large, rough substrates, we observed that most crystals nucleated at low supersaturation and then grew steadily and at rate in proportion to ice supersaturation values. At temperatures below −30 °C, we repeatedly observed crystals where growth became completely stalled, even at moderate supersaturations (> 115 % RH_i) that had previously induced growth in that crystal and continued to lead to growth in adjacent cystals. This stalled growth was only observed following a specific cycle of humidity adjustment: the excess vapor supply of a steadily growing crystal was gradually reduced until reaching equilibrium, with observable growth ceasing, and with no sublimation apparent. This equilibrium condition was held for 1–5 min, after which the vapor pressure was gradually increased (or temperature decreased) until RH_i exceeded equilibrium by a few percent. In many instances, the original crystal would not resume growth, even though adjacent crystals continued to nucleate and grow. Figure 3 provides time-separated panels illustrating one such event were a crystal held at equilibrium failed to grow following a 0.3 °C decrease in temperature, despite several nearby crystals nucleating and growing. (see Supplement videos for an additional example). We interpret this an example of side-by-side ice crystals subject to 2 different surface conditions: (a) one where steady growth

ACPD
14, 8393–8418, 2014

continues at emergent dislocations or stacking faults, likely partly induced by the underlying substrate and (b) one where a previously rough surface has been reconditioned by the momentary maintainence of equilbrium vapor pressure, leaving the surface to grow only by 2-D nucleation requiring vapor in excess of a critical supersaturation. The stalled crystal surfaces do not appear to be completely absent of mesoscopic roughness, nor are they observably different than the growing surfaces, implying that the surface condition differentiating separate growth mechanisms is determined at a smaller scale than observable here. The observation of growth at dislocations and 2-D nucleations would not be unprecentended – Sazaki et al. (2010) used interference-contrast microscopy to demonstrate depositional growth in ice via both 2-D layer nucleation and spiral growth steps at screw dislocations. Several recent studies have also suggested that ice Ic/ice Ih combinations may play an important role in ice formation at temperatures up to 243 K, particularly for small particles (Murray and Bertram, 2006; Malkin et al., 2012). Kuhs et al. (2010) present data suggesting that ice Ic sequences may be implicated in stacking faults of ice being deposited at these temperatures, and that ice Ic should be expected to present a rougher surface and lead to macroscopic psuedo-hexagonal structures. Their neutron-diffraction studies also demonstrate that ice-Ic anneals toward ice-Ih with increasing time and temperature. Both of these findings are consistent with the steady growth we observe at low supersaturation as well as the occurence of inhibited growth when the surface is given the opportunity to anneal emergent stacking faults.

3.2 Sublimating crystals

In many instances, cycling of vapor pressure was conducted to observe the sensitivity of surface topography to ambient humidity. In the portions of the cycle below equilibrium vapor pressure, a significantly different character to the surface roughness was observed. Instead of regular or spreading ridges, plateaus, and steps, we observed concave, scalloped depressions away from the original surface. In the case of polycrystalline examples (Fig. 4a), the scalloped depressions took on especially dramatic

ACPD
14, 8393–8418, 2014

shapes near former grain boundaries, with sharp peaks often evident during advanced sublimation. However, even single-crystal examples did produce marked scalloping (Fig. 4b–d), which often initiated at the site of roughness produced during previous growth. Furthermore, if the supersaturation was once again increased above equilibrium, the crystal would typically exhibit micro-faceting that initiated along the ridges bounding adjacent sublimation-scallops (Supplement video).

3.3 Transported crystals

As described in Sect. 2.2, ice crystals where grown at low supersaturation, at −50 °C, and at ambient lab pressure in an external, freezer-based diffusion chamber and subsequently captured and transported to the ESEM cold stage in a sealed small-volume cell, with conditions maintained at ice/vapor equilbrium until imaging could commence. The goal of this test was to compare the character of suface roughness observed in experiements described in Sects. 3.1 and 3.2 with ice crystals grown in conditions more closely approximating cirrus clouds. While not completely isolated like an ice crystal floating in air, the crystals grown in the freezer-chamber grew outward from a fiber, differentiating them from the close substrate contact seen with ESEM-grown crystals. The presence of large partial pressures of Nitrogen and Oxygen provides the other important departure from ESEM-grown crystals. The particle-scale habits and aspect ratios are in agreement with measurements by Bailey and Hallet (2004). The habits are qualitatively more elongated than the more tabular crystals typically observed in ESEM. The surfaces themselves (Fig. 5) clearly exibit signatures of mesoscopic roughening that are similar to examples of roughness seen in ESEM-grown crystals. However, for most transported crystals, the crystal edges are more intricate that those observed in ESEM and portions of surfaces of some transported crystals do appear smooth even at magnification greater than 1000×, a rare observation in our ESEM-grown crystals. While we took efforts to maintain equilibrium conditions between capture and imaging, we still can not say with certainty that the crystals were not exposed to some variation in RH_i during transport. The transported crystals hint at some significant differences in

ACPD
14, 8393–8418, 2014

roughness morphology, but they do provide evidence that crystals grown in air/water mixtures and with minimal support also exhibit mesocopic roughness with similarity to that observed in ESEM-grown crystals.

4 Conclusions

The ESEM images of ice in Sect. 3 confirms the observations on the nature of mesoscopic roughness recently described by several studies (Neshyba et al., 2013; Ulanowski et al., 2013; Pfalgraff et al., 2010; Pedersen et al., 2011; Zimmerman, 2007) and also reveals additional patterns of roughness morpology at high magnification, across a wide range of temperatures, on crystal basal facets, sublimating crystals, and crystals grown in air/water vapor mixtures. Light microscopy has generated highly-detailed images of ice crystals (Libbrecht, 2005; Walden et al., 2003), but a combination of working distance constraints, diffraction limits to resolution, and transmitted light illumination have conspired to prevent visible imaging of mesoscopic surface features. We suggest that submicron scale roughness can also be obscured to detection by ESEM imaging, where the probability of resolving mesoscopic surface topography depends on a combination of factors including the size and depth of the features themselves, the magnification and resolution of the micrograph, the brightness and contrast, and the orientation of the ice crystal with respect to the viewing angle. When brightness and contrast are adjusted to optimal levels, increasing the magnification and resolution serves to create a detailed portrait of ice crystal mesoscopic surfaces which in turn can increase the calculated roughness measure $\langle r \rangle$. Furthermore, high magnification images near 10 000× (Fig. 6) depict significant roughness on spatial scales below 200 nm, indicating that for modeling of roughness-induced scattering changes, it is not sufficient to consider light scattering only in the geometric optics regime.

Because the ice crystals shown here were grown both inside the pure vapor environment of the ESEM and in external air/vapor mixtures, the ubiquitous presence of mesoscopic roughness indicates that the roughening mechanisms are not caused by

ACPD
14, 8393–8418, 2014

the ESEM environment alone and are likely to be significant in atmospheric ice. This observation appears to be well-aligned with a growing body of evidence (Baran, 2012; Baum et al., 2011; Ulanowski et al., 2006; Yang et al., 2008) suggesting that measured scattering functions from ice crystals fit a rough surface model more successfully than crystals with presumed smooth-faceted surfaces. Despite strong similarity in the subjective appearance of roughness morphologies, there do also appear to be significant differences in overal crystal habit, intricacy of crystal edges, as well as some diffence in the patterns of mesoscopic roughness. To increase the utility of these observations, these differences should be investigated further and analyzed quantitatively.

We believe that these new observations of prevalent surface topography in ice crystals warrant careful consideration in the scattering models that are used for satellite retrievals of cirrus ice microphysics, and in turn, affect the radiative modeling of cirrus clouds in climate models. Furthermore, the ubiquity of a complex mesoscopic landscape on the surface of ice crystals also has potential wide-ranging impacts to theories of charge transfer in thunderstorms, the heteogeneous chemistry of stratospheric ozone, and the sintering of ice crystals in snowpacks and glaciers. We suggest that the next steps should focus on efforts to examine and quantify roughness in crystals transported from cirrus-analog environments and development of a mixed air/vapor capability for ice crystal growth in ESEM.

Supplementary material related to this article is available online at http://www.atmos-chem-phys-discuss.net/14/8393/2014/acpd-14-8393-2014-supplement.zip.

Acknowledgements. The authors thank J. Poirier at the Princeton Image and Analysis Center for essential technical assistance with ESEM imaging. Research support was generously provided by the Research Corporation Cottrell College Science Award 19914, NASA EPOESS grant #10-0047, and The College of New Jersey

ACPD
14, 8393–8418, 2014

References

Bailey, M. and Hallett, J.: Growth Rates and Habits of Ice Crystals between −20° and −70°C, J. Atmos. Sci., 61, 514–554, 2004.

Baran, A. J.: From the single-scattering properties of ice crystals to climate prediction: a way forward, Atmos. Res., 112, 45–69, 2012.

Baum, B. A., Yang, P., Hu, Y., and Feng, Q.: The impact of ice particle roughness on the scattering phase matrix, J. Quant. Spectrosc. Ra., 111, 2534–2549, 2010.

Baum, B. A., Yang, P., Heymsfield, A. J., Schmitt, C. G., Xie, Y., Bansemer, A., Hu, Y., J., and Zhang, Z.: Improvements in shortwave scattering and absorption models for the remote sensing of ice clouds, J. Appl. Meteorol. Clim., 50, 1037–1056, 2011.

Bennett, H. E. and Porteus, J. O.: Relation between surface roughness and specular reflectance at normal incidence, J. Opt. Soc. Am., 51, 123–129, 1961.

Blackford, J. R.: Sintering and microstructure of ice: a review, J. Phys. D Appl. Phys., 40, R355, doi:10.1088/0022-3727/40/21/R02, 2007.

Bony, S., Colman, R., Kattsov, V. M., Allan, R. P., Bretherton, C. S., Dufresne, J.-L., Hall, A., Hallegatte, S., Holland, M. M., Ingram, W., Randall, D. A., Soden, B. J., Tselioudis, G., and Webb, M.: How well do we understand and evaluate climate change feedback processes?, J. Climate, 19, 3445–3482, 2006.

Bryant, G. W., Hallett, J., and Mason, B. J.: The epitaxial growth of ice on single-crystalline substrates, J. Phys. Chem. Solids, 12, 189–195, 1960.

Burkhardt, U. and Kärcher, B.: Global radiative forcing from contrail cirrus, Nature Climate Change, 1, 54–58, 2011.

Cole, B., Yang, P., Baum, B. A., Riedi, J., and C.-Labonnote, L.: Ice particle habit and surface roughness derived from PARASOL polarization measurements, Atmos. Chem. Phys. Discuss., 13, 29483–29519, doi:10.5194/acpd-13-29483-2013, 2013.

Connolly, P., Flynn, M., Ulanowski, Z., Chourlatan, T. W., Gallagher, M., and Bower, K. N.: Calibration of the cloud particle imager probes using calibration beads and ice crystal analogs: the depth of field, J. Atmos. Ocean. Tech., 24, 1860–1879, 2007.

Cotton, R., Osborne, S. Ulanowski, Z., Hirst, E., Kaye, P. H., and Greenaway, R. S.: The ability of the small ice detector, SID-2 to characterize cloud particle and aerosol morphologies obtained during flights of the FAAM BAe-146 research aircraft, J. Atmos. Ocean. Tech., 27, 290–303, 2010.

ACPD
14, 8393–8418, 2014

Dash, J. G., Mason, B. L., and Wettlaufer, J. S.: Theory of charge and mass transfer in ice–ice collisions, J. Geophys. Res., 106, 20395–20402, 2001.
Furukawa, Y., Yamamoto, M., and Kuroda, T. Ellipsometric study of the transition layer on the surface of an ice crystal, J. Cryst. Growth, 82, 665–677, 1987.
Garrett, T. J., Gerber, H., Baumgardner, D. G., Twohy, C. H., and Weinstock, E. M.: Small, highly reflective ice crystals in low-latitude cirrus, Geophys. Res. Lett., 30, 2132, doi:10.1029/2003GL018153, 2003.
Gierens, K. M., Monier, M., and Gayet, J.-F.: The deposition coefficient and its role for cirrus clouds, J. Geophys. Res., 108, 4059–4063, 2003.
Harrington, J. Y., Lamb, D., and Carver, R.: Parameterization of surface kinetic effects for bulk microphysical models: influences on simulated cirrus dynamics and structure, J. Geophys. Res., 114, D06212, doi:10.1029/2008JD011050, 2009.
Heymsfield, A. J., Schmitt, C., Bansemer, A, Van Zadelhoff, G. J., McGill, M. J., Twohy, C., and Baumgardner, D.: Effective radius of ice cloud particle populations derived from aircraft probes, J. Atmos. Ocean. Tech., 23, 361–380, 2006.
IPCC: Climate Change – Contribution of Working Group I to the Fourth Assessment Report of the IPCC, Cambridge University Press, Cambridge, 2007.
Jensen, E. J., Lawson, P., Baker, B., Pilson, B., Mo, Q., Heymsfield, A. J., Bansemer, A., Bui, T. P., McGill, M., Hlavka, D., Heymsfield, G., Platnick, S., Arnold, G. T., and Tanelli, S.: On the importance of small ice crystals in tropical anvil cirrus, Atmos. Chem. Phys., 9, 5519–5537, doi:10.5194/acp-9-5519-2009, 2009.
Kahnert, M., Sandvik, A. D., Biryulina, M., Stamnes, J. J., and Stamnes, K.: Impact of ice particle shape on short-wave radiative forcing: a case study for an arctic ice cloud, J. Quant. Spectrosc. Ra., 109, 1196–1218, 2008.
Krämer, M., Schiller, C., Afchine, A., Bauer, R., Gensch, I., Mangold, A., Schlicht, S., Spelten, N., Sitnikov, N., Borrmann, S., de Reus, M., and Spichtinger, P.: Ice supersaturations and cirrus cloud crystal numbers, Atmos. Chem. Phys., 9, 3505–3522, doi:10.5194/acp-9-3505-2009, 2009.
Kuhs, W. F., Sippel, C., Falenty, A., and Hansen, T. C.: Extent and relevance of stacking disorder in “ice Ic”, P Natl. Acad. Sci. USA, 109, 21259–21264, 2012.
Kuroda, T. and Lacmann, R.: Growth kinetics of ice from the vapour phase and its growth forms, J. Cryst. Growth, 56, 189–205, 1982.

ACPD
14, 8393–8418, 2014

Lamb, D. and Hobbs, P. V.: Growth rates and habits of ice crystals grown from the vapor phase, J. Atmos. Sci., 28, 1506–1509, 1971.
Lamb, D.: Crystal growth: 2-D or not 2-D?, in: Proc. of 13th Inter. Conf. on Clouds and Precip., Reno, NV, 1221–1224, 14–18 August, 2000.
Libbrecht, K.: The physics of snow crystals, Rep. Prog. Phys., 68, 855–895, doi:10.1088/0034-4885/68/4/R03, 2005.
Magee, N., Moyle, A. M., and Lamb, D.: Experimental determination of the deposition coefficient of small cirrus-like ice crystals near −50 °C, Geophys. Res. Lett., 33, L17813, doi:10.1029/2006GL026665, 2006.
Malkin, T. L., Murray, B. J., Brukhno, A. V., Anwar, J., and Salzmann, C. G.: Structure of ice crystallized from supercooled water, P. Natl. Acad. Sci. USA, 109, 1041–1045, doi:10.1073/pnas.1113059109, 2012.
Mauno, P., McFarquhar, G. M., Räisänen, P., Kahnert, M., Timlin, M. S., and Nousiainen, T.: The influence of observed cirrus microphysical properties on shortwave radiation: a case study over Oklahoma, J. Geophys. Res., 116, D22208, doi:10.1029/2011JD016058, 2011.
McFarquhar, G. M., Um, J., Freer, M., Baumgardner, D., Kok, G. L., and Mace, G.: Importance of small ice crystals to cirrus properties: observations from the Tropical Warm Pool International Cloud Experiment, TWP-ICE, Geophys. Res. Lett., 34, L13803, doi:10.1029/2007GL029865, 2007.
McNeill, V. F., Geiger, F. M., Loerting, T., Trout, B. L., Molina, L. T., and Molina, M. J.: Interaction of hydrogen chloride with ice surfaces: the effects of grain size, surface roughness, and surface disorder, J. Phys. Chem. A, 111, 6274–6284, 2007.
Mitchell, D. L., Rasch, P., Ivanova, D., McFarquhar, G., and Nousiaine, T.: Impact of small ice crystal assumptions on ice sedimentation rates in cirrus clouds and GCM simulation, Geophys. Res. Lett., 35, L09806, doi:10.1029/2008GL033552, 2008.
Murray, B. J. and Bertram, A. K.: Formation and stability of cubic ice in water droplets, Phys. Chem. Chem. Phys., 8, 186–192, 2006.
Nelson, J. and Knight, C.: Snow crystal habit changes explained by layer nucleation, J. Atmos. Sci., 55, 1452–1464, 1998.
Neshyba, S. P., Lowen, B., Benning, M., Lawson, A., and Rowe, P. M.: Roughness metrics of prismatic facets of ice, J. Geophys. Res.- Atmos., 3309–3318, doi:10.1002/jgrd.50357, 2013.
Pedersen, C., Mihranyan, A., and Stromme, M.: Surface transition on ice induced by the formation of a grain boundary, PLoS one, 6, e24373, doi:10.1371/journal.pone.0024373, 2011.

ACPD
14, 8393–8418, 2014

Peter, T., Marcolli, C., Spichtinger, P., Corti, T., Baker, M. B., and Koop, T.: When dry air is too humid, Science, 314, 1399–1402, 2006.
Pfalzgraff, W. C., Hulscher, R. M., and Neshyba, S. P.: Scanning electron microscopy and molecular dynamics of surfaces of growing and ablating hexagonal ice crystals, Atmos. Chem. Phys., 10, 2927–2935, doi:10.5194/acp-10-2927-2010, 2010.
Saunders, C. P. R.: Thunderstorm electrification laboratory experiments and charging mechanisms, J. Geophys. Res., 99, 10773–10779, 1994.
Sazaki, G., Zepeda, S., Nakatsubo, S., Yokoyama, E., and Furukawa, Y.: Elementary steps at the surface of ice crystals visualized by advanced optical microscopy, P. Natl. Acad. Sci. USA, 107, 19702–19707, 2010.
Schnaiter, M., Kaye, P. H., Hirst, E., Ulanowski, Z., and Wagner, R.: Exploring the surface roughness of small ice crystals by measuring high resolution angular scattering patterns, AAPP, 89, C1V89S1P084, doi:10.1478/C1V89S1P084, 2011.
Shcherbakov, V., Gayet, J. F., Backer, B., and Lawson, P.: Light scattering by single natural ice crystals, Am. Meteorol. Soc., 63, 1513–1525, 2006.
Sun, W., Hu, Y., Lin, B., Liu, Z., and Videen, G.: The impact of ice cloud particle microphysics on the uncertainty of ice water content retrievals, J. Quant. Spectrosc. Ra., 112, 189–196, 2011.
Ulanowski, Z., Hesse, H., Kaye, P. H., Baran, A. J.: Light scattering by complex ice-analogue crystals, J. Quant. Spectrosc. Ra., 100, 382–392, doi:10.1016/j.jqsrt.2005.11.052, 2006.
Ulanowski, Z., Hirst, E., Kaye, P. H., and Greenaway, R.: Retrieving the size of particles with rough and complex surfaces from two-dimensional scattering patterns, J. Quant. Spectrosc. Ra., 113, 2457–2464, doi:10.1016/j.jqsrt.2012.06.019, 2012.
Ulanowski, Z., Kaye, P. H., Hirst, E., and Greenaway, R. S.: Light scattering by ice particles in the Earth's atmosphere and related laboratory measurements, in: Procs. 12th Int. Conf. on Electromagnetic and Light Scattering: ELS'XII, 28 June–2 July 2010, Helsinki, Finland, 294–297, 2010.
Um, J. and McFarquhar, G. M.: Dependence of the single-scattering properties of small ice crystals on idealized shape models, Atmos. Chem. Phys., 11, 3159–3171, doi:10.5194/acp-11-3159-2011, 2011.
Walden, V. P., Warren, S. G., and Tuttle, E.: Atmospheric ice crystals over the antarctic plateau in winter, Am. Meteorol. Soc., 42, 1391–1405, 2003.

ACPD
14, 8393–8418, 2014

Wergin, W. P., Rango, A., and Erbe, E. F.: Observations of snow crystals using low-temperature scanning electron microscopy, Scanning, 17, 41–49, 1995.
Yang, H., Dobbie, S., Herbert, R., Connolly, P., Gallagher, M., Ghosh, S., Al-Jumur, S. M. R. K., and Clayton, J.: The effect of observed vertical structure, habits, and size distributions on the solar radiative properties and cloud evolution of cirrus clouds, Q. J. Roy. Meteor. Soc., 138, 1221–1232, 2012.
Yang, P. and Liou, K. N.: Single-scattering properties of complex ice crystals in terrestrial atmosphere, Contr. Atmos. Phys., 71, 223–248, 1998.
Yang, P., Hong, G., Kattawar, G., Minnis, P., and Hu, Y.: Uncertainties associated with the surface texture of ice particles in satellite-based retrieval of cirrus clouds: Part II – Effect of particle surface roughness on retrieved cloud optical thickness and effective particle size, IEEE T. Geosci. Remote, 46, 1948–1957, 2008.
Yang, P., Bi, L., Baum, B. A., Liou, K. N., Kattawar, G. W., Mishchenko, M. I., and Cole, B.: Spectrally consistent scattering, absorption, and polarization properties of atmospheric ice crystals at wavelengths from 0.2 to 100 µm, J. Atmos. Sci., 70, 330–347, 2013.
Yi, B., Yang, P., Baum, B. A., L'Ecuyer, T., Oreopoulos, L., Mlawer, E. J., Heymsfield, A. J., and Liou, K. N.: Influence of ice particle surface roughening on the global cloud radiative effect, J. Atmos. Sci., 70, 2794–2807, doi:10.1175/JAS-D-13-020.1, 2013.
Zimmermann, F., Ebert, M., Worringen, A., Schutz, L., and Weinbruch, S.: Environmental scanning electron microscopy, ESEM as a new technique to determine ice nucleation capability of individual atmospheric particles, Atmos. Environ., 41, 8219–8227, 2007.

ACPD
14, 8393–8418, 2014

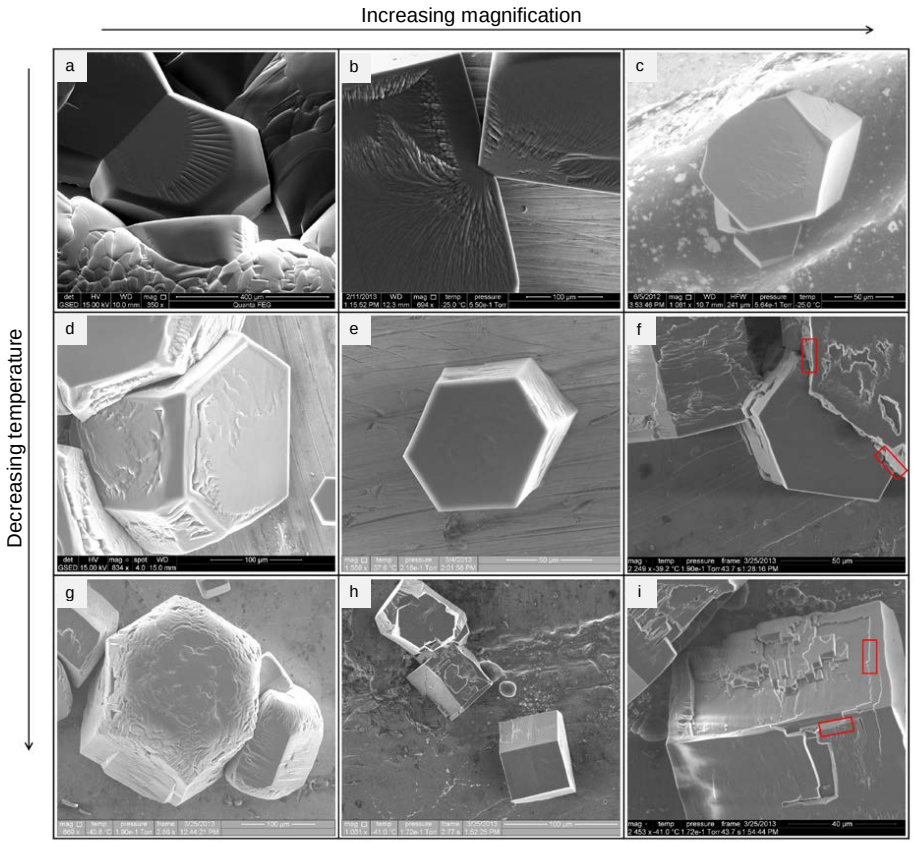

Fig. 1. Image panels at a variety of magnification, temperatures, pressures – all showing various examples of mesoscopic surface topography. Red rectangles in **(f)** and **(i)** show sites used for calculating roughness measure $\langle r \rangle$.

ACPD
14, 8393–8418, 2014

Mesoscopic surface roughness of ice crystals pervasive

N. B. Magee et al.

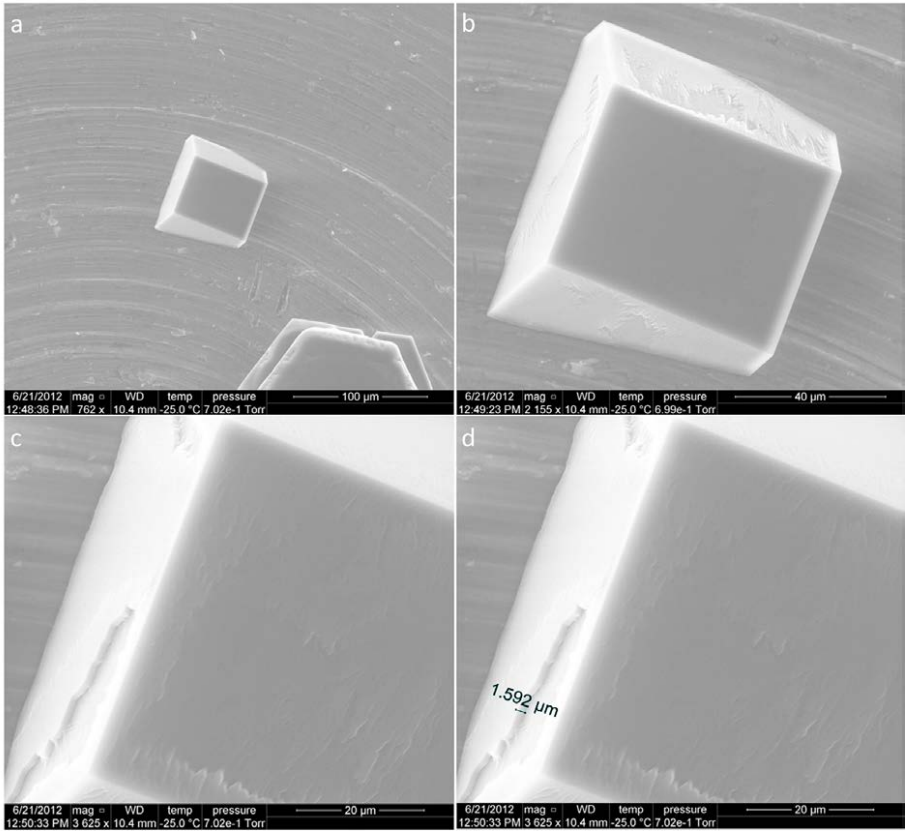

Fig. 2. Demonstration of increased magnification effect upon perceived roughness is shown here, as well as a measurement of ridge depth **(d)**.

ACPD
14, 8393–8418, 2014

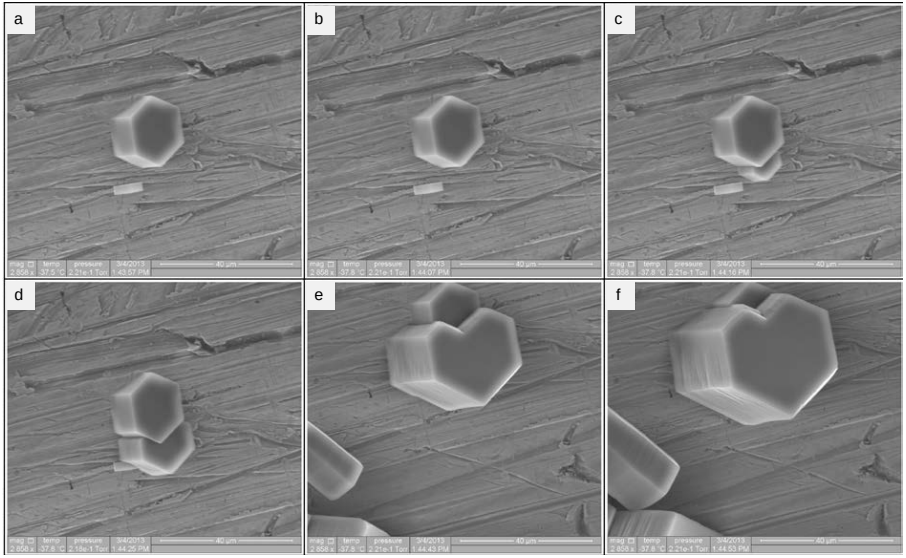

Fig. 3. Series of frames separated by ∼ 10 s (20 s between **d** and **e** as the acquisition was re-centered to capture growing crystals at bottom-left in **d** and **e**). The orignal 2 crystals at equilibrium in **(a)** do not grow when subjected to a temperature decrease of 0.3 °C (equivalent to ∼ 105 RH_i), with vapor pressure held constant.

ACPD
14, 8393–8418, 2014

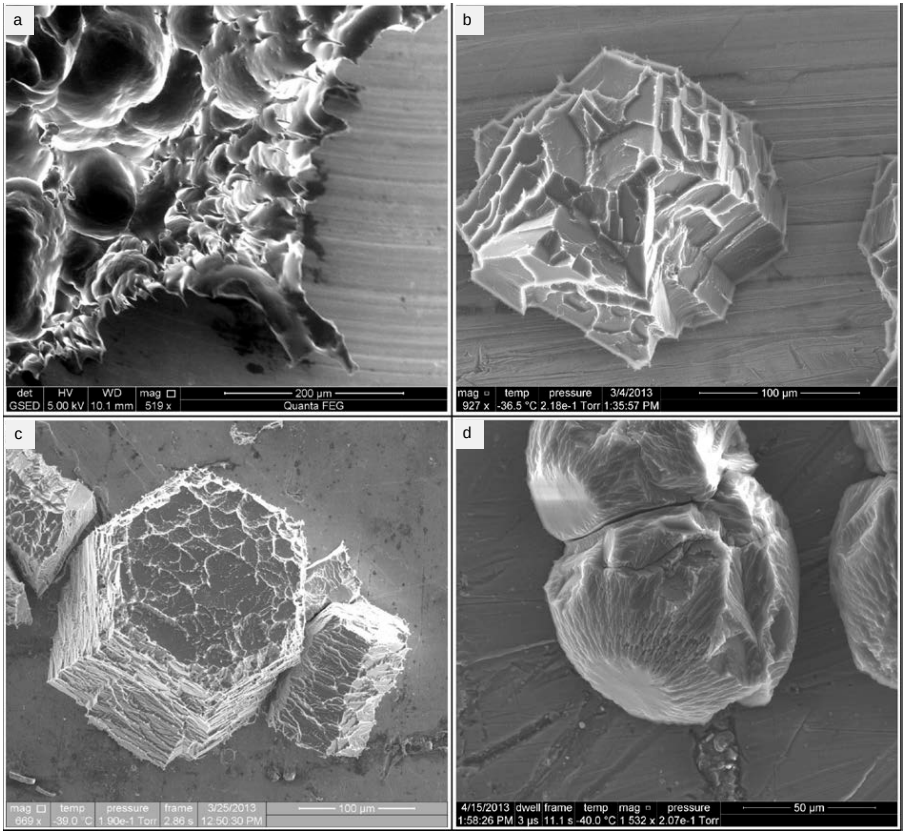

Fig. 4. Sublimating ice crystals displaying scallopped depressions and sharp ridges and peaks of roughness. **(a)** was originally composed of a polycrystalline ice particle, with peaks and ridges prominent at former grain boundaries.

ACPD
14, 8393–8418, 2014

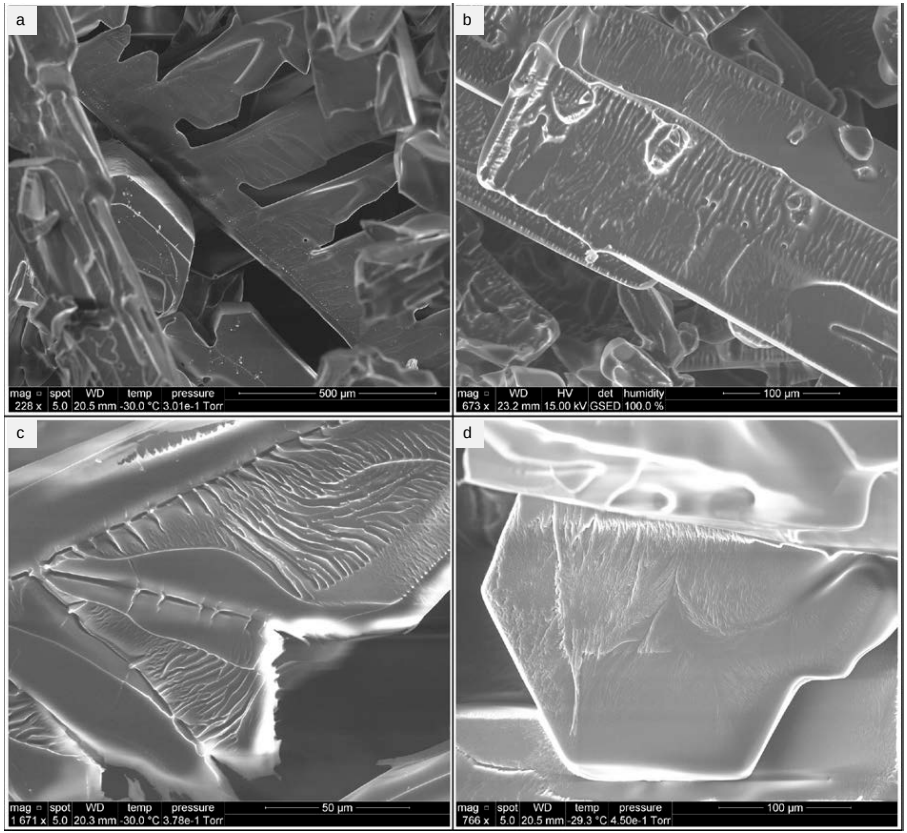

Fig. 5. Transported ice crystals.

ACPD
14, 8393–8418, 2014

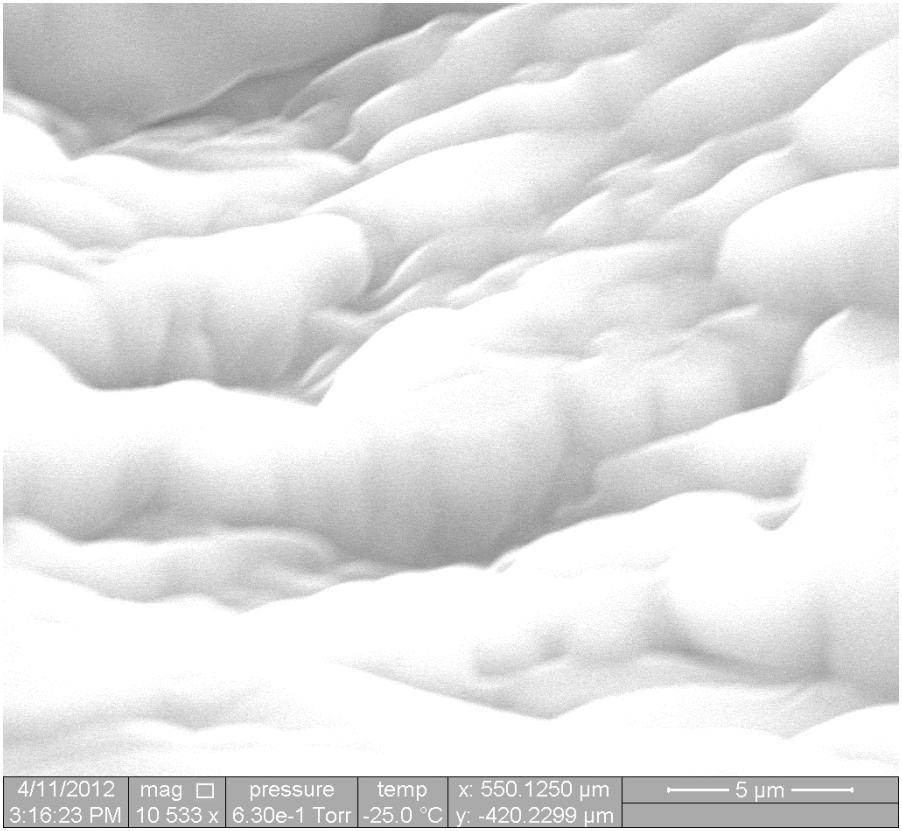

Fig. 6. Ice crystals are observed at high magnification, the highest we were able to attain without sacrificing the quality of the image.

ACPD
14, 8393–8418, 2014